CSP-AIT-Net: A contrastive learning-enhanced spatiotemporal graph attention framework for short-term metro OD flow prediction with asynchronous inflow tracking

Yichen Wang

Division of Logistics and Transportation, Tsinghua University, 100084 Beijing, China

Email: wang-yc22@mails.tsinghua.edu.cn

Chengcheng Yu (Corresponding author)

Urban Mobility Institute, Tongji University, 200092 Shanghai, China

Email: chengchengyu@tongji.edu.cn

Abstract: Accurate origin-destination (OD) passenger flow prediction is crucial for enhancing metro system efficiency, optimizing scheduling, and improving passenger experiences. However, current models often fail to effectively capture the asynchronous departure characteristics of OD flows and underutilize the inflow and outflow data, which limits their prediction accuracy. To address these issues, we propose CSP-AIT-Net, a novel spatiotemporal graph attention framework designed to enhance OD flow prediction by incorporating asynchronous inflow tracking and advanced station semantics representation. Our framework restructures the OD flow prediction paradigm by first predicting outflows and then decomposing OD flows using a spatiotemporal graph attention mechanism. To enhance computational efficiency, we introduce a masking mechanism and propose asynchronous passenger flow graphs that integrate inflow and OD flow with conservation constraints. Furthermore, we employ contrastive learning to extract high-dimensional land use semantics of metro stations, enriching the contextual understanding of passenger mobility patterns. Validation of the Shanghai metro system demonstrates improvement in short-term OD flow prediction accuracy over state-of-the-art methods. This work contributes to enhancing metro operational efficiency, scheduling precision, and overall system safety.

Keywords: OD passenger flow, short-term prediction, asynchronous inflow tracking, contrastive learning, spatiotemporal graph attention, station semantics

1. Introduction

Metro systems provide efficient, high-capacity transit solutions that reduce surface congestion and promote sustainable urban mobility (Lin *et al.*, 2022; C. Yang *et al.*, 2023). However, managing these systems presents significant challenges, particularly in balancing fluctuating passenger demand with service capacity, reducing station

congestion, and optimizing daily scheduling (Mandhani *et al.*, 2021; Teng *et al.*, 2020; Xu *et al.*, 2020). Effective management of these challenges is essential to ensure the reliability and attractiveness of metro services, maintain daily operations, and enhance the passenger experience (Mo *et al.*, 2019).

One promising approach to addressing these operational issues is the accurate prediction of metro passenger flows (Fang *et al.*, 2019; Liu *et al.*, 2019). Accurate flow predictions, supported by *Automated Fare Collection (AFC)* systems, *Mobility as a Service (MaaS)* applications, and *artificial intelligence (AI)* algorithms, are critical for effective resource allocation, improved service scheduling, and reduced delays (Fang *et al.*, 2023; Hasselwander *et al.*, 2022; Liu *et al.*, 2022). Accurate short-term OD flow predictions can help prevent station overcrowding during peak hours, directly improving passenger satisfaction (Hoogervorst *et al.*, 2020; Ma *et al.*, 2019).

Metro passenger flow prediction research can be classified based on prediction level and granularity (Tang *et al.*, 2019). Short-term predictions are particularly valuable for managing daily operations, ensuring that resources are optimally deployed to meet fluctuating demand (Chen *et al.*, 2022; Du *et al.*, 2022). Predictions can also focus on either the station level or the origin-destination (OD) level, each with distinct operational uses (Ou *et al.*, 2023).

The primary research approaches for metro passenger flow prediction can be categorized into two paradigms: sequence-based and feature-based methods (Huang *et al.*, 2023; Tang *et al.*, 2019). Sequence-based models like time-series methods are effective in capturing temporal dependencies but often fail to account for external factors influencing passenger demand (Zhao *et al.*, 2020). Feature-based models leverage machine learning to incorporate these factors, offering more flexibility (Shi

et al., 2020). More recently, spatiotemporal deep learning methods have shown promise in capturing complex spatial and temporal dependencies within metro systems (Lu *et al.*, 2021; Y. Yang *et al.*, 2023; Zeng and Tang, 2023).

Despite recent advancements, several challenges remain. Current models typically fail to integrate inflow, outflow, and OD flows, missing opportunities to leverage these relationships to enhance prediction accuracy. Additionally, the asynchronous nature of passenger flows between OD pairs is often overlooked, as shown in Fig 1. Finally, there is a need for more selective identification of relevant spatiotemporal correlations to improve prediction performance.

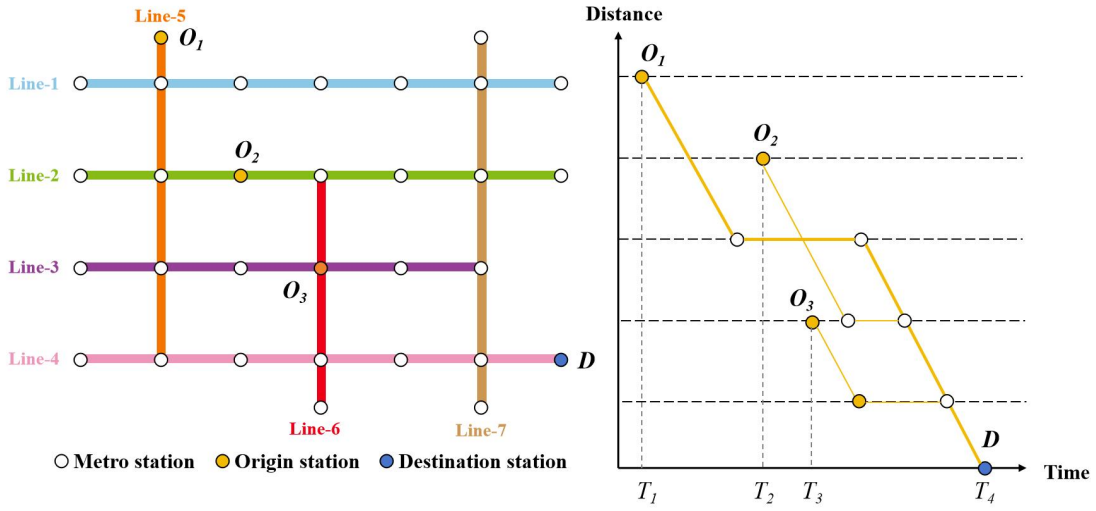

Fig. 1. Illustration of asynchronous passenger flow.

This paper proposes CSP-AIT-Net to address these challenges, proposing a novel framework that integrates station embeddings from contrastive learning, asynchronous passenger flow graphs, and a spatiotemporal graph attention mechanism. This framework aims to enhance the accuracy and robustness of metro passenger flow prediction. Specifically, we propose: (1) a contrastive learning approach to model complex station semantics, (2) asynchronous flow graphs to capture varying OD travel durations, and (3) a spatiotemporal attention mechanism that focuses on the most relevant spatial and temporal dependencies. The framework is validated through

a case study of Shanghai's metro system, demonstrating its effectiveness in improving prediction accuracy and robustness compared to traditional methods.

The remainder of this paper is organized as follows: Section 2 reviews the related work on station-level and OD-level forecasting methods. Section 3 introduces the key concepts, the problem statement, and relevant background algorithms. Section 4 details the architecture of the CSP-AIT-Net model and its components. Section 5 presents the case study, parameter settings, and comparison algorithms. Section 6 analyzes the experimental results, including model performance and outcomes from ablation studies. Section 7 discusses the limitations and suggests directions for future research.

2. Related works

2.1 Station-level prediction methods

The prediction of metro passenger flow has evolved significantly, beginning with statistical approaches during the early stages of research (Yan *et al.*, 2018). Statistical methods, such as the autoregressive integrated moving average (ARIMA), Kalman filter, and generalized autoregressive conditional heteroskedasticity (GARCH) models, utilized historical ridership data to forecast demand by capturing autocorrelations and temporal volatility (Chen *et al.*, 2020; Jiao *et al.*, 2016). While these models effectively predicted short-term trends, they were limited in their ability to capture the nonlinear dynamics inherent in metro systems, and their computational efficiency suffered with the introduction of larger datasets (Fang *et al.*, 2022).

Machine learning approaches were adopted to overcome these limitations, offering the capability to model complex, nonlinear relationships without predefined assumptions (Toqué *et al.*, 2017). Techniques such as artificial neural networks

(ANN), support vector regression (SVR), and decision trees improved prediction accuracy (Roos *et al.*, 2017; Shi *et al.*, 2020; Wei and Chen, 2012). However, these methods struggled with capturing temporal dependencies, which are crucial in predicting fluctuating passenger flows, particularly when real-time predictions are required (Wang *et al.*, 2020).

The increasing complexity of metro systems necessitated methods that could capture intricate temporal dependencies, leading to the adoption of deep learning models such as Long Short-Term Memory (LSTM) networks and Gated Recurrent Units (GRU) (Liu *et al.*, 2019). These models excelled in retaining long-term temporal patterns, thus enhancing the accuracy of dynamic flow predictions (Chen *et al.*, 2022; Ma *et al.*, 2024). Furthermore, hybrid models that integrated LSTMs with Convolutional Neural Networks (CNNs) proved effective in capturing both spatial and temporal features of passenger flow data, allowing simultaneous learning from spatial correlations and temporal trends (Du *et al.*, 2020; Zhang *et al.*, 2021).

Recently, Graph Neural Networks (GNNs) have emerged as powerful tools for modeling non-Euclidean spatial relationships between metro stations (Yin *et al.*, 2023). GNNs, including Graph Convolutional Networks (GCNs) and Graph Attention Networks (GATs), have demonstrated considerable improvements by dynamically weighting the importance of inter-station relationships (Cheng *et al.*, 2024). These models, especially when combined with temporal modules in frameworks like Spatial-Temporal Graph Convolutional Networks (ST-GCNs), have shown promise in jointly modeling spatial and temporal dependencies (Ma *et al.*, 2024; Zhan *et al.*, 2024).

2.2 OD-level prediction methods

Predicting origin-destination (OD) passenger flows in metro systems presents

unique challenges compared to station-level flow forecasting (Huang *et al.*, 2023; Wei and Chen, 2012). The summary of methods for OD-level metro passenger flow prediction is shown in Table 1. Unlike station-level models that focus on forecasting ridership at individual stations, OD flow prediction aims to estimate passenger movement between specific station pairs, typically within short time intervals (Su *et al.*, 2024; Y. Yang *et al.*, 2023). This requires modeling interactions across the entire network, influenced by both temporal patterns and spatial factors, which significantly increases the complexity (Li *et al.*, 2019; Yang *et al.*, 2022).

One of the primary challenges is modeling the dynamic relationships between OD pairs, where interactions depend on both network structure and temporal variations (Lu *et al.*, 2023). Unlike localized station-level traffic patterns, OD-level models must consider the complete network structure and the temporal dependencies that arise from daily and weekly travel patterns (Zhan *et al.*, 2024). The complexity of OD prediction is compounded by the incomplete or unavailable nature of OD matrices in real-time, particularly in large transit systems (Liu *et al.*, 2019).

Recent OD-level prediction methods have focused on incorporating advanced spatiotemporal models to address these challenges. The multi-view passenger flow model introduced by Zheng *et al.* (2023) separately learns station-level and cross-station dynamics, utilizing GATs and GRUs. By integrating real-time data such as inflows and outflows, it has demonstrated a 2.5% improvement in WMAPE compared to traditional methods, highlighting the importance of inter-station interactions.

Beyond spatiotemporal modeling, integrating diverse data sources has been another focus area. Su *et al.* (2024) proposed the high-dimensional feature fusion deep learning (HDF-DL) model, which incorporates external data such as weather

conditions and land use features. By clustering OD pairs, the model reduces prediction complexity, particularly for systems with large numbers of OD pairs.

Despite significant advancements, several challenges remain in OD-level prediction methods as metro systems expand. Scalability is a persistent issue, especially given the increasing complexity of urban transit networks. Lu *et al.* (2021) addressed this by proposing a dual-attention graph neural network (DAGNN), which effectively captured both inbound and outbound relationships between stations, enhancing inter-station modeling capabilities. While DAGNN improved prediction accuracy, its computational requirements still pose challenges for high-dimensional OD matrices. As networks grow, ensuring these methods maintain efficiency under larger, more dynamic conditions remains an area needing further exploration.

Data sparsity is another key challenge in OD-level prediction, often resulting from incomplete OD matrices due to asynchronous passenger movement records. Jiang *et al.* (2022) tackled this issue with a deep learning framework using LSTM networks to reconstruct missing data and capture temporal dependencies, which significantly improved prediction accuracy. However, irregularities in OD data continue to present difficulties, particularly for real-time and large-scale applications. Addressing data gaps effectively in evolving transit environments thus remains a critical focus.

Incorporating flow conservation principles further complicates OD prediction. Accurate modeling requires that system entries match exits, a complexity not fully addressed by traditional models. Liu *et al.* (2023) made progress in this area with a dual information transformer, which captured mutual causality between OD and DO flows, enhancing consistency and accuracy. However, explicitly incorporating flow conservation across large-scale transit networks remains challenging. This paper seeks

to bridge these gaps.

Table 1. Spatiotemporal modeling methods for OD-level metro passenger flow prediction research.

Author/Year	Method	Temporal Dependency	Spatial Dependency	Empirical Case	Key Findings
Xu *et al.* (2023)	Adaptive Feature Fusion Network (AFFN)	Multi-task learning for inflow and outflow prediction	Multiple knowledge-based graphs, hidden correlations	Nanjing, Xi'an, China	AFFN improves OD prediction by fusing spatial dependencies adaptively and addressing data sparsity.
Zhang *et al.* (2023)	Spatiotemporal Convolutional Neural Network (STCNN)	Temporal Convolutional Neural Network (TCN)	OD pair importance calculation,	Chengdu, China	STCNN achieves high accuracy for critical OD pairs by focusing on capacity utilization.
Shen *et al.* (2024)	Spatial-Temporal Dynamic Attentive Multi-Hypergraph Network (ST-DAMHGN)	Attention mechanism for dynamic information synthesis	Multi-hypergraph representation, perceptual field extraction	Hangzhou, China	Hypergraph structure effectively captures correlations without physical road networks.
Yang *et al.* (2022)	Spatiotemporal Virtual Graph Convolutional Network (ST-VGCN)	Gated Recurrent Units (GRU) for temporal learning	Virtual graph using Pearson correlation	Shenzhen, China	Virtual graphs efficiently model OD relationships and handle data sparsity.
Su *et al.* (2024)	High-Dimensional Feature Fusion Deep Learning (HDF-DL)	Temporal module for trend and cyclic pattern capture	K-means and K-shape clustering of OD pairs	Large-scale Metro in China	HDF-DL accurately captures temporal variations and integrates external features for higher accuracy.
Lv *et al.* (2024)	Passenger Source Attention Mechanism CNN (PSAM-CNN)	Temporal sequence learning using attention mechanism	Spatial attention focused on oversaturated sections	Shenzhen, China	PSAM-CNN effectively predicts OD flows causing oversaturation, aiding in congestion management.
Jiang *et al.* (2022)	LSTM-Based Deep Learning Framework	Multiple LSTMs for short- and long-term temporal dependencies	Temporally shifted graph matrix for spatial correlations	Hong Kong MTR	The reconstruction mechanism handles partial OD observations, improving accuracy.
Lu *et al.*	Dual	Temporal	Inbound and	Beijing,	DAGNN effectively

(2021)	Attentive Graph Neural Network (DAGNN)	attention integrated with sequence decoder	outbound graph representations	China	captures both inbound and outbound flows, detecting emergencies.
Liu *et al.* (2023)	Heterogeneous Information Aggregation Machine (HIAM)	Seq2Seq framework with dual transformer for OD/DO learning	Joint OD and DO ridership modeling	Shanghai, China	HIAM integrates incomplete OD and DO data, enhancing prediction performance.
Li *et al.* (2019)	Spatial-Temporal Correlation Model	Nonlinear regression to handle emergency fluctuations	Passenger flow fluctuation analysis based on AFC data	Beijing, China	Accurately predicts OD flows during emergencies, supporting effective evacuation strategies.
Shen *et al.* (2021)	Hybrid Model (Gravity + CNN-AE)	Modified Gravity Model for trend detection	Convolutional autoencoder to capture spatial patterns	Beijing, China	The hybrid approach balances interpretability with accuracy, outperforming time-series models.

3. Preliminaries

This section defines the key concepts and notations employed in the study, formally articulates the metro OD passenger flow prediction task and provides an overview of the background algorithms that underpin the proposed methodology.

3.1 Notions and definitions

Definition 1: Time interval. The time interval represents a specific segment of the day used for temporal discretization. The entire day is divided evenly into T time intervals, each of duration ΔT, where $\Delta T \in \{10, 20, 30, 60\}$ minutes; $t \in \boldsymbol{T} = \{1, 2, \ldots, T\}$ denote the index for each interval, where t represents a distinct period within the day.

Definition 2: Metro network. The metro network is modeled as an undirected graph $\boldsymbol{G} = (\boldsymbol{V}, \boldsymbol{E})$, where $\boldsymbol{V} = \{v_1, v_2, ..., v_N\} \in R^N$ is the set of nodes, each representing a station, and N is the total number of stations. $\boldsymbol{E} = \{e_{ij}\} \in R^{N \times N}$ is the set of edges,

each representing a direct operating line between stations v_i and v_j. If there exists an operating line between stations v_i and v_j, then an edge $e_{ij} \in \boldsymbol{E}$.

Definition 3: Origin-Destination (OD) Trip. The OD trip $\boldsymbol{v}$ describes the complete journey of a passenger through the metro system, including all relevant attributes:

- $\boldsymbol{v}^o \in \boldsymbol{V}$: The origin station from which the passenger begins their journey.
- $\boldsymbol{v}^{t_o} \in \boldsymbol{T}$: The interval when the passenger enters the origin station.
- $\boldsymbol{v}^d \in \boldsymbol{V}$: The destination station at which the passenger leaves the train.
- $\boldsymbol{v}^{t_d} \in \boldsymbol{T}$: The interval when the passenger exits the destination station.

The trips are recorded by the *Automatic Fare Collection (AFC)* system, which logs the entry and exit data for passengers.

Definition 4: Station-level inflow and outflow. The station-level inflow and outflow describe the movement of passengers entering or leaving a particular station during a given time interval.

- Inflow $\boldsymbol{\phi}_t^{(i)}$ for station $v_i \in \boldsymbol{V}$ at time interval $t \in \boldsymbol{T}$ is defined as the total number of passengers entering station v_i during interval t:

$$\boldsymbol{\phi}_t^{(i)} = \sum\nolimits_{\boldsymbol{v}} \Theta\left(\boldsymbol{v}^{t_o} = t \wedge \boldsymbol{v}^o = v_i\right), \forall v_i \in \boldsymbol{V} \tag{1}$$

  where $\Theta(\cdot)$ is an indicator function equal to 1 if the condition is met, and 0 otherwise. The inflows across all stations during time interval t can be represented as a vector:

$$\boldsymbol{\phi}_t = \left[\boldsymbol{\phi}_t^{(1)}, \boldsymbol{\phi}_t^{(2)}, \ldots, \boldsymbol{\phi}_t^{(N)}\right] \in R^N, \forall t \in \boldsymbol{T} \tag{2}$$

- Outflow $\boldsymbol{\psi}_q^{(i)}$ for station $v_i \in \boldsymbol{V}$ at time interval $t \in \boldsymbol{T}$ is defined as the number of passengers leaving station v_i during the interval t:

$$\psi_t^{(i)} = \sum_{\upsilon} \Theta\left(\upsilon^{t_d} = t \wedge \upsilon^{d} = v_i\right), \forall v_i \in V \tag{3}$$

The outflows across all stations at time interval t are represented as a vector:

$$\psi_t = \left[\psi_t^{(1)}, \psi_t^{(2)}, ..., \psi_t^{(N)}\right] \in R^N, \forall t \in T \tag{4}$$

Definition 5: OD passenger flow matrix. The OD passenger flow matrix $P_t \in R^{N \times N}$ at time interval $t \in T$ represents the number of passengers traveling between origin-destination (OD) station pairs. Specifically, $p_t^{(ij)}$ represents the number of passengers departing from station v_i and arriving at station v_j during time interval t:

$$p_t^{(ij)} = \sum_{\upsilon} \Theta\left(\upsilon^{t_d} = t \wedge \upsilon^{o} = v_i \wedge \upsilon^{d} = v_j\right), \forall t \in T, \forall v_i, v_j \in V, v_i \neq v_j \tag{5}$$

where the OD passenger flow matrix P_t encapsulates the spatial distribution of passenger flows for every station pair during time interval t.

Definition 6: Asynchronous OD inflow and outflow. Due to differing travel times between origin and destination stations, asynchronous OD inflow represents the temporal discrepancy in the inflow and outflow observations for different OD pairs. Define τ_{ij} as the average travel time between origin station $v_i \in V$ and destination station $v_j \in V$. The asynchronous inflow tensor is represented by:

$$A_t^{(ij)} = \sum_{\tau=t-\tau_{ij}-\Delta t}^{t-\tau_{ij}+\Delta t} \phi_\tau^{(i)}, \forall t \in T, v_i, v_j \in V \wedge v_i \neq v_j \tag{6}$$

The relationship indicates that inflows recorded at an earlier time interval $t - \tau_{ij}$ (with a buffer time interval $\Delta\tau$) result in outflows at a later time interval t, reflecting the average travel time between stations.

Definition 7: Land use semantics. The land use semantics vector s_i for station

$v_i \in \boldsymbol{V}$ captures important land-use features in the surrounding area which may impact passenger flow. The POI intensity is defined as the number of Points of Interest (POI) within a radius of the station:

- $\gamma_{res}^{(i)}$: Number of residential-related POIs.
- $\gamma_{work}^{(i)}$: Number of work-related POIs.
- $\gamma_{com}^{(i)}$: Number of commercial and entertainment-related POIs.
- $\gamma_{edu}^{(i)}$: Number of educational-related POIs.
- $\gamma_{med}^{(i)}$: Number of medical-related POIs.

Other indicators are dummy variables which indicate the specific land use type:

- $\eta_{CBD}^{(i)}$: Whether the metro station is proximity to the Central Business District (CBD).
- $\eta_{Uni}^{(i)}$: Whether the metro station is in proximity to the university.
- $\eta_{Hub}^{(i)}$: Whether the metro station is in proximity to the transportation hub.
- $\eta_{\mathrm{Cen}}^{(i)}$: Whether the metro station is located within the city center.

The station's land use semantics are expressed as:

$$\boldsymbol{s}_i = \left[\gamma_{res}^{(i)}, \gamma_{work}^{(i)}, \gamma_{rec}^{(i)}, \gamma_{edu}^{(i)}, \gamma_{med}^{(i)}, \eta_{CBD}^{(i)}, \eta_{Uni}^{(i)}, \eta_{Hub}^{(i)}, \eta_{Cen}^{(i)} \right] \in R^{N \times d_1}, \forall v_i \in \boldsymbol{V} \tag{7}$$

where d_1 represents the feature dimension.

3.2 Problem statement

Given the metro network $\boldsymbol{G} = (\boldsymbol{V}, \boldsymbol{E})$, the land use semantics $\boldsymbol{s}_i$ for each station $v_i \in \boldsymbol{V}$, and the historical OD passenger flow $\boldsymbol{p}_t \in R^{N \times N}$ for past time intervals $t \in \boldsymbol{T}$, our goal is to predict the OD-level passenger flows $\boldsymbol{p}_{t+1} \in R^{N \times N}$ for a future target

interval $t+1$.

The prediction task must account for two key constraints:

1. **Asynchronous passenger flow constraint:** Due to varying travel times τ_{ij} between different origin-destination pairs, the OD flow predictions must consider the temporal misalignment between inflows and corresponding outflows.
2. **Inflow consistency constraint:** The aggregated OD passenger flow must be consistent with the originating inflows, ensuring passenger conservation across the network.

Formally, the metro OD passenger flow prediction task can be expressed as learning a deep learning function $F(\cdot)$ such that:

$$\boldsymbol{p}_{t+1}^{(ij)} = F\left(\boldsymbol{G}, \{\boldsymbol{s}_i\}_{i=1}^{N}, \{\boldsymbol{p}_{\tau}^{(ij)}\}_{\tau\in[1,t]}\right), \forall v_i, v_j \in \boldsymbol{V} \wedge v_i \neq v_j \tag{8}$$

where $F(\cdot)$ utilizes the graph structure $\boldsymbol{G}$, the land use attributes $\boldsymbol{s}_i$, and historical OD data to predict the OD passenger flows for the future time interval $t+1$, while considering asynchronous and inflow consistency constraints.

3.3 Background algorithm knowledge

This section provides an overview of two algorithms that support the station-level outflow prediction: Graph Attention Networks (GAT) for capturing spatial relationships between stations and Long Short-Term Memory (LSTM) networks for learning temporal dependencies of passenger flows.

3.3.1 GAT for station-level spatial dependency

GAT are utilized to learn the spatial dependencies among metro stations by utilizing an attention mechanism that assigns varying importance to neighboring

nodes. The input feature matrix is denoted by $\boldsymbol{X} \in R^{N \times d_1}$, where each feature vector $\boldsymbol{x}_i \in R^{d_1}$ corresponds to station v_i with feature dimension d_1. The GAT mechanism can be summarized as attention calculation, normalization and node feature update. For each station v_i, an unnormalized attention score $\boldsymbol{e}_{ij}$ is computed for each neighboring station $v_j \in \boldsymbol{M}_i$:

$$\boldsymbol{e}_{ij} = LeakyReLU\left(\boldsymbol{a}^T \times \left[\boldsymbol{W}_{GAT}\boldsymbol{x}_i \,||\, \boldsymbol{W}_{GAT}\boldsymbol{x}_j\right]\right) \tag{9}$$

where $\boldsymbol{W}_{GAT} \in R^{d_1 \times d_1}$ is the learnable weight and $\boldsymbol{a}^T \in R^{2 \times d_1}$ is the attention vector. The scores are normalized using the SoftMax function:

$$\boldsymbol{\alpha}_{ij} = \frac{exp\left(\boldsymbol{e}_{ij}\right)}{\sum_{v_k \in \boldsymbol{M}_i} exp\left(\boldsymbol{e}_{ik}\right)} \tag{10}$$

The updated feature $\boldsymbol{x}_i^{(l+1)}$ at layer l is obtained by aggregating neighboring features using the normalized attention scores:

$$\boldsymbol{x}_i^{(l+1)} = \sigma\left(\sum_{j \in \boldsymbol{M}_i} \boldsymbol{\alpha}_{ij}\boldsymbol{W}_{GAT}\boldsymbol{x}_j\right) \tag{11}$$

where $\sigma(\cdot)$ is a non-linear activation function. The GAT model allows to dynamically focus on more influential stations, which helps in accurately modeling the spatial relationships that affect station-level outflows.

3.3.2 LSTM for temporal dependency

LSTMs can learn both short-term and long-term temporal patterns in sequences of passenger flows. It maintains hidden state $\boldsymbol{h}_t$ and a cell state $\boldsymbol{c}_t$ to retain memory. Specifically, the forget gate $\boldsymbol{f}_t$ determines the extent to which the previous cell state $\boldsymbol{c}_{t-1}$ is retained:

$$\boldsymbol{f}_t = \sigma\left(\boldsymbol{W}_f\boldsymbol{x}_t + \boldsymbol{U}_f\boldsymbol{h}_{t-1} + \boldsymbol{b}_f\right) \tag{12}$$

The input gate $\boldsymbol{\kappa}_t$ controls the flow of new information into the cell state, and the candidate cell state $\tilde{\boldsymbol{c}}_t$ is calculated as follows:

$$\boldsymbol{\kappa}_t = \sigma\left(\boldsymbol{W}_\kappa \boldsymbol{x}_t + \boldsymbol{U}_\kappa \boldsymbol{h}_t + \boldsymbol{b}_\kappa\right) \tag{13}$$

$$\tilde{\boldsymbol{c}}_t = tanh\left(\boldsymbol{W}_c \boldsymbol{x}_t + \boldsymbol{U}_c \boldsymbol{h}_t + \boldsymbol{b}_c\right) \tag{14}$$

The cell state $\boldsymbol{c}_t$ is updated by combining the previous cell state $\boldsymbol{c}_{t-1}$ with the new candidate state $\tilde{\boldsymbol{c}}_t$, modulated by the forget and input gates:

$$\boldsymbol{c}_t = \boldsymbol{f}_t \odot \boldsymbol{c}_{t-1} + \kappa_t \odot \tilde{\boldsymbol{c}}_t \tag{15}$$

where $\odot$ denotes element-wise multiplication. The output gate $\boldsymbol{o}_t$ generates the hidden state $\boldsymbol{h}_t$:

$$\boldsymbol{o}_t = \sigma\left(\boldsymbol{W}_o \boldsymbol{x}_t + \boldsymbol{U}_o \boldsymbol{h}_{t-1} + \boldsymbol{b}_o\right) \tag{16}$$

$$\boldsymbol{h}_t = \boldsymbol{o}_t \odot tanh\left(\boldsymbol{c}_t\right) \tag{17}$$

where $\boldsymbol{W}_f$, $\boldsymbol{W}_\kappa$, $\boldsymbol{W}_c$, $\boldsymbol{W}_o$ are weight matrices for the gates, and $\boldsymbol{U}_f$, $\boldsymbol{U}_\kappa$, $\boldsymbol{U}_c$, $\boldsymbol{U}_o$ are matrices for the hidden state. The hidden state $\boldsymbol{h}_t$ encodes temporal dependencies of the passenger flow and could be utilized in the following prediction process.

4. Methodology

The proposed CSP-AIT-Net framework consists of four components: contrastive learning-enhanced station semantic extraction, outflow prediction and asynchronous inflow tracking, spatiotemporal graph attention mechanism for outflow decomposition, and joint loss of OD flow prediction accuracy and inflow constraints. The workflow of CSP-AIT-Net framework is shown in Figure 2.

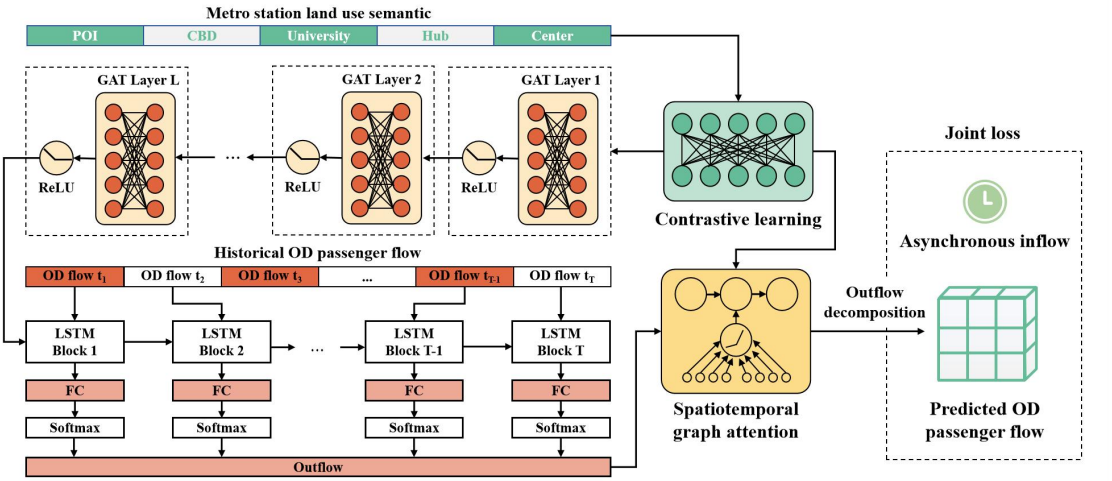

Fig. 2. Workflow of the proposed CSP-AIT-Net framework.

4.1 Contrastive learning-enhanced station semantic extraction

Contrastive learning is utilized to generate high-dimensional semantic embeddings for each metro station, deriving a robust feature vector for each station. For a metro network $\boldsymbol{G}=(\boldsymbol{V},\boldsymbol{E})$ consisting of N metro stations denoted by the set $\boldsymbol{V}=\{v_1,v_2,...v_N\}$, the semantic attribute vector $\boldsymbol{s}_i \in R^{d_1}$ is defined, including POI characteristics (work, residential, commercial, educational, medical-related POI intensity) and location dummy variables (whether the metro station is near to central business district, university, transportation hub or located in the suburban areas). The feature matrix representing all stations is expressed as:

$$\boldsymbol{S}=\left[\boldsymbol{s}_1,\boldsymbol{s}_2,...,\boldsymbol{s}_N\right]^T \in R^{N\times d_1} \tag{18}$$

The contrastive learning is then utilized to project the semantic attributes into a higher-dimensional embedding space $\boldsymbol{z}_i \in R^{d_2}$ where $d_2 > d_1$. To generate the embedding vector $\boldsymbol{z}_i$,the positive station pair $\left(v_i,v_j^+\right)$ and negative station pair $\left(v_i,v_k^-\right)$ are firstly identified based on the daily outflows sequence, denoted as:

$$\boldsymbol{\psi}_i=\left[\boldsymbol{\psi}_1^{(i)},\boldsymbol{\psi}_2^{(i)},...,\boldsymbol{\psi}_t^{(i)}\right]^T \in R^T, \forall v_i \in \boldsymbol{V} \tag{19}$$

where T represents the number of time intervals throughout the day, and $\boldsymbol{\psi}^{(i)}$ represents the outflow at station v_i. The cosine similarity between the outflow sequences of two stations v_i and v_j is defined as:

$$sim\left(\boldsymbol{\psi}^{(i)},\boldsymbol{\psi}^{(j)}\right)=\frac{\boldsymbol{\psi}^{(i)T}\boldsymbol{\psi}^{(j)}}{\left\|\boldsymbol{\psi}^{(i)}\right\|\left\|\boldsymbol{\psi}^{(j)}\right\|},\forall v_i,v_j\in\boldsymbol{V}\wedge v_i\neq v_j \tag{20}$$

Then the station pairs are classified into positive pair or negative pair based on the following conditional rules:

$$\left(v_i,v_j\right)\in\begin{cases}P\ , & if\ \ sim(\boldsymbol{\psi}^{(i)},\boldsymbol{\psi}^{(j)})>\varepsilon_1\\ N\ , & if\ sim(\boldsymbol{\psi}^{(i)},\boldsymbol{\psi}^{(j)})<\varepsilon_2\end{cases} \tag{21}$$

where P represents the set of positive pairs, N represents the set of negative pairs, ε_1 and ε_2 are similarity threshold parameters.

Define $\boldsymbol{z}_i$, $\boldsymbol{z}_j^+$ and $\boldsymbol{z}_k^-$ as the embeddings of station v_i, the positive corelated station v_j^+ and the negative correlated station v_j^-, the contrastive loss for a given station v_i is defined as:

$$\mathrm{L}_i=-log\frac{exp\left(sim\left(\boldsymbol{z}_i,\boldsymbol{z}_j^+\right)/\varpi\right)}{exp\left(sim\left(\boldsymbol{z}_i,\boldsymbol{z}_j^+\right)/\varpi\right)+\sum_{k=1}^{|\boldsymbol{N}|}\exp\left(sim\left(\boldsymbol{z}_i,\boldsymbol{z}_k^-\right)/\varpi\right)},\forall v_i\in\boldsymbol{V} \tag{22}$$

where ϖ represents the parameter controlling the sharpness of the distribution. $|\boldsymbol{N}|$ is the number of negative samples for each anchor-positive pair, $exp(\cdot)$ is the exponential function used to ensure non-negative similarity scores. The overall contrastive loss is defined as:

$$L=\frac{1}{N}\sum_{i=1}^{N}L_i \tag{23}$$

After training the embedding function, the high-dimensional semantic

embeddings $z_i \in R^{d_2}$ for each station v_i are obtained:

$$\boldsymbol{Z} = \left[z_1, z_2, ..., z_N\right]^T \in R^{N \times d_2} \tag{24}$$

These embeddings serve as the station-level input features for downstream station-level and OD-level passenger flow prediction tasks.

4.2 Outflow prediction and asynchronous inflow tracking

The outflow prediction task combined GAT and LSTM to obtain station-level outflow for future time intervals. GAT is constructed on the metro graph $\boldsymbol{G} = (\boldsymbol{N}, \boldsymbol{V})$ and updates each station's embedding vectors $z_i \in R^{d_2}$ by aggregating from neighboring nodes. As described in section 3.3, the attention coefficient α_{ij} between station v_i and v_j is computed as:

$$\alpha_{ij} = \frac{exp\left(LeakyReLU\left(\boldsymbol{a}^T \times \left[\boldsymbol{W}_{GAT} z_i \,||\, \boldsymbol{W}_{GAT} z_j\right]\right)\right)}{\sum_{v_k \in \boldsymbol{M}_i} exp\left(LeakyReLU\left(\boldsymbol{a}^T \times \left[\boldsymbol{W}_{GAT} z_i \,||\, \boldsymbol{W}_{GAT} z_k\right]\right)\right)} \tag{25}$$

where $\boldsymbol{W}_{GAT} \in R^{d_2 \times d_3}$ represents the learnable weight matrix, $\boldsymbol{a} \in R^{2d_2}$ is an attention vector, $\boldsymbol{M}_i$ represents the set of neighbors of station v_i. The updated embedding for station v_i is then given by:

$$z_i' = \sigma\left(\sum_{j \in \boldsymbol{M}_i} \alpha_{ij} \boldsymbol{W}_{GAT} z_i\right) \tag{26}$$

where $\sigma(\cdot)$ is a non-linear activation function such as ReLU. The temporal dynamics of the outflow at each station are captured with LSTM network, where historical outflow sequence is utilized to produce latent representation $\boldsymbol{H}_t$ at interval t:

$$\boldsymbol{H}_t = LSTM\left(\boldsymbol{\psi}_t\right), \forall t \in \boldsymbol{T} \tag{27}$$

The GAT-updated embedding $\boldsymbol{Z}' \in R^{N \times d_2}$ and the LSTM-generated hidden state

$\boldsymbol{H}_t \in R^{N\times d_3}$ are concatenated to form a joint representation:

$$\boldsymbol{u}_t = \left[\boldsymbol{Z}' \,\|\, \boldsymbol{H}_t\right], t \in \boldsymbol{T} \tag{28}$$

Then the station-level outflow $\boldsymbol{\psi}_{t+1}^{(i)}$ for the next time interval $t+1$ is predicted using a fully connected layer $\Gamma(\cdot)$:

$$\widehat{\boldsymbol{\psi}}_{t+1} = \Gamma\left(\boldsymbol{u}_t\right) \tag{29}$$

Asynchronous inflow tracking is an analytical approach which trace the passenger sources across different time intervals. It leverages the known inflow during current time interval as prior knowledge to enhance the accuracy of subsequent outflow decomposition task. The asynchronous inflow tensor is denoted by $\boldsymbol{A} \in R^{N\times N\times T}$. Specifically, the asynchronous inflow between origin v_i and destination v_j during interval t is defined as:

$$\boldsymbol{A}_t^{(ij)} = \sum_{\tau=t-\tau_{ij}-\Delta t}^{t-\tau_{ij}+\Delta t} \boldsymbol{\phi}_\tau^{(i)}, \forall t \in \boldsymbol{T}, v_i, v_j \in \boldsymbol{V} \wedge v_i \neq v_j \tag{30}$$

where $\boldsymbol{\phi}_\tau^{(i)}$ donate the inflow at station v_i during interval τ, $\tau_{ij} \in N$ represents the average travel time between stations v_i and v_j, $\Delta t \in N$ denotes the buffer period. The asynchronous inflow contributes to eliminate infeasible OD allocations, enhancing the robustness and accuracy of the subsequent outflow decomposition task.

4.3 Spatiotemporal graph attention mechanism for outflow decomposition

The spatiotemporal graph attention mechanism is proposed to effectively decompose predicted outflows into detailed origin-destination (OD) flows. The input includes a historical OD flow tensor $\boldsymbol{P} \in R^{N\times N\times T}$. Additionally, the predicted outflows at each station for a future time interval $t+1$ are denoted as $\boldsymbol{\psi}_{t+1} \in R^N$. The adaptive mask $\boldsymbol{M} \in R^{N\times N\times T}$ regulates the attention contribution of origin-destination pairs.

The spatial attention mechanism is applied to the historical OD tensor to generate an updated representation of the OD relationships between stations. For each OD pair (v_i, v_j), the attention coefficient $\boldsymbol{\alpha}_{ijk}^t$ is computed to capture the importance of neighboring OD pairs (v_i, v_j) on the pair (v_k, v_j) at time t:

$$\boldsymbol{\alpha}_{ijk}^t = \frac{exp\left(LeakyReLU\left(\boldsymbol{a}^T \cdot \left[\boldsymbol{W}_\alpha \boldsymbol{y}_{ij}^t \| \boldsymbol{W}_\alpha \boldsymbol{y}_{kj}^t\right]\right)\right)}{\sum_{v_k \in V_i} exp\left(LeakyReLU\left(\boldsymbol{a}^T \cdot \left[\boldsymbol{W}_\alpha \boldsymbol{y}_{ij}^t \| \boldsymbol{W}_\alpha \boldsymbol{y}_{kj}^t\right]\right)\right)}, \forall v_i, v_j, v_k \in \boldsymbol{V}, t \in \boldsymbol{T} \wedge v_i \neq v_j \quad (31)$$

where $\boldsymbol{\alpha}_{ijk}^t$ is a learnable weight matrix that transforms input features into a latent space, $\boldsymbol{y}_{ij}^t$ is the embedded representation initialized by historical OD passenger flow time series. $\boldsymbol{a}$ is the weight vector used to compute the attention score. $\|$ represents concatenation function. Using these attention coefficients, the updated representation $\left(\boldsymbol{y}_{ij}^t\right)'$ for OD pair (v_i, v_j) at time t is obtained through:

$$\left(\boldsymbol{y}_{ij}^t\right)' = \sum_{v_k \in V_i} \boldsymbol{\alpha}_{ijk}^t \cdot \boldsymbol{W}_{\boldsymbol{\alpha}} \boldsymbol{y}_{kj}^t, \forall v_i, v_j, v_k \in \boldsymbol{V}, t \in \boldsymbol{T} \wedge v_i \neq v_j \quad (32)$$

The temporal attention mechanism is subsequently used to incorporate information from prior time intervals, thus enabling modeling of the temporal dependencies. The temporal attention coefficient $\boldsymbol{\beta}_{ij}^{t_1 t_2}$ of time interval t_1 on time interval t_2 for each OD pair (v_i, v_j) is calculated as follows:

$$\boldsymbol{\beta}_{ij}^{t_1 t_2} = \frac{exp\left(LeakyReLU\left(\boldsymbol{b}^T \cdot \left[\boldsymbol{W}_\beta \boldsymbol{y}_{ij}^{t_1} \| \boldsymbol{W}_\beta \boldsymbol{y}_{ij}^{t_2}\right]\right)\right)}{\sum_{t_3 < t_2} exp\left(LeakyReLU\left(\boldsymbol{W}_\beta \boldsymbol{y}_{ij}^{t_3} \| \boldsymbol{W}_\beta \boldsymbol{y}_{ij}^{t_2}\right)\right)}, \forall v_i, v_j \in \boldsymbol{V}, t_1, t_2 \in \boldsymbol{T} \wedge v_i \neq v_j \wedge t_1 < t_2 \quad (33)$$

where $\boldsymbol{W}_\beta \in R^{d_3 \times d_3}$ is a learnable weight matrix for temporal feature transformation. $\boldsymbol{b} \in R^{2 \times d_3}$ is a weight vector for computing temporal attention scores. The temporal aggregation results in an updated temporal representation $\left(\boldsymbol{y}_{ij}^t\right)''$:

$$\left(\boldsymbol{y}_{ij}^{t}\right)^{''}=\sum_{t_1<t}\boldsymbol{\beta}_{ij}^{t_1 t}\cdot\boldsymbol{W}_{\beta}\boldsymbol{y}_{ij}^{t},\forall v_i,v_j\in\boldsymbol{V},t\in\boldsymbol{T}\wedge v_i\neq v_j \tag{34}$$

The combined representation $\boldsymbol{\theta}_{ij}^{t}$ for OD pair $\left(v_i,v_j\right)$ at time t is derived by concatenating both spatial and temporal representations:

$$\boldsymbol{\theta}_{ij}^{t}=\left[\left(\boldsymbol{y}_{ij}^{t}\right)^{'}\|\left(\boldsymbol{y}_{ij}^{t}\right)^{''}\right],\forall v_i,v_j\in\boldsymbol{V},t\in\boldsymbol{T}\wedge v_i\neq v_j \tag{35}$$

The resulting tensor $\boldsymbol{\theta}\in R^{N\times N\times T}$ is utilized, together with the similarity coefficient matrix $\boldsymbol{\rho}\in R^{N\times N}$, to predict the probability distribution for OD flow decomposition. The similarity coefficient is derived from GAT with the station semantic embeddings:

$$\boldsymbol{\rho}_{ij}=GAT\left(\boldsymbol{z}_i,\boldsymbol{z}_j\right),\forall v_i,v_j\in\boldsymbol{V}\wedge v_i\neq v_j \tag{36}$$

The decomposition probability for OD flow at time interval $t+1$ is determined as:

$$\boldsymbol{\xi}_{ij}^{t+1}=softmax\left(\left(\boldsymbol{W}_{\boldsymbol{\rho}}\boldsymbol{\rho}_{ij}+\boldsymbol{W}_{\boldsymbol{SP}}\cdot\boldsymbol{\theta}_{ij}^{t}\right)\cdot\boldsymbol{m}_{ij}^{t}\right),\forall v_i,v_j\in\boldsymbol{V},t\in\boldsymbol{T}\wedge v_i\neq v_j,\boldsymbol{m}_{ij}^{t}\in\{0,1\} \tag{37}$$

where $\boldsymbol{W}_{\boldsymbol{\rho}}$ and $\boldsymbol{W}_{\boldsymbol{SP}}$ are learnable weights, $\boldsymbol{m}_{ij}^{t}$ is the adaptive mask that regulates the influence of station v_i on destination v_j at interval t, dynamically updated during model training. Then the predicted OD flow $\widehat{\boldsymbol{\psi}}_{t+1}^{(i)}$ for time interval $t+1$ is obtained by multiplying the decomposition probability with the predicted outflow:

$$\widehat{\boldsymbol{p}}_{ij}^{t+1}=\boldsymbol{\xi}_{ij}^{t+1}\times\boldsymbol{\psi}_{j}^{t+1},\forall v_i,v_j\in\boldsymbol{V},t\in\boldsymbol{T}\wedge v_i\neq v_j \tag{38}$$

By employing the spatiotemporal graph attention mechanism, the approach can effectively leverage both spatial and temporal relationships between stations, decomposing outflows into OD flows.

4.4 Joint loss of OD flow prediction accuracy and inflow constraints

A joint loss function is introduced that balances both the OD passenger flow prediction accuracy and consistency with actual inflow. The asynchronous inflow tracking process utilizes the predicted OD flows for time $t+1$ to calculate the corresponding inflows at each origin station. Given that different OD pairs have varying average travel times, denoted by τ_{ij} for an OD pair from station v_i to station v_j, the relevant inflow can be determined by:

$$\widehat{\boldsymbol{A}}_{t+1}^{(i)} = \sum_{j=1}^{N} \sum_{\tau=t+1-\tau_{ij}-\Delta t}^{t+1-\tau_{ij}+\Delta t} \widehat{\boldsymbol{P}}_{ij}^{\tau}, \forall v_i \in \boldsymbol{V}, t \in \boldsymbol{T} \tag{39}$$

The inflow constraint loss is expressed as:

$$L_{Inflow} = \frac{1}{N} \times \frac{1}{T} \times \sum_{t=1}^{T} \sum_{i=1}^{N} \left(\widehat{\boldsymbol{A}}_{t+1}^{(i)} - \boldsymbol{A}_{t+1}^{(i)} \right)^2 \tag{40}$$

The OD flow prediction loss is defined as:

$$L_{OD} = \frac{1}{N^2} \times \frac{1}{T} \times \sum_{i=1}^{N} \sum_{j=1}^{N} \sum_{t=1}^{T} \left(\widehat{\boldsymbol{p}}_{ij}^{t+1} - \boldsymbol{p}_{ij}^{t+1} \right)^2 \tag{41}$$

The overall joint loss function combines these two components to ensure both prediction accuracy and inflow consistency:

$$L_{Joint} = \lambda_{OD} \cdot L_{Joint} + \lambda_{Inflow} \cdot L_{Inflow} \tag{42}$$

5. Experiment

5.1 Dataset preparation

The dataset used in this study consists of OD-level passenger flow data from the Shanghai metro system, collected over a three-week period from September 1 to September 21, 2023. Data were recorded at 10-minute intervals during standard metro

operational hours (6:00 AM to 10:00 PM), providing a high temporal resolution of passenger movements. This period was selected to exclude holidays and other special dates, focusing solely on typical operational patterns. The dataset was split into 14 training days and 7 validation days, allowing for a balanced evaluation of model performance. Data from 409 metro stations across Shanghai were used, providing comprehensive coverage of the network and representing a diverse set of origin-destination (OD) pairs.

The outflow at different time intervals on weekdays and weekends are shown in Fig 3. and Fig 4. The outflow on weekdays follows a bimodal distribution characteristic of commuting patterns, while the weekend outflow only shows an evening peak, with the peak time being later than the morning peak on weekdays.

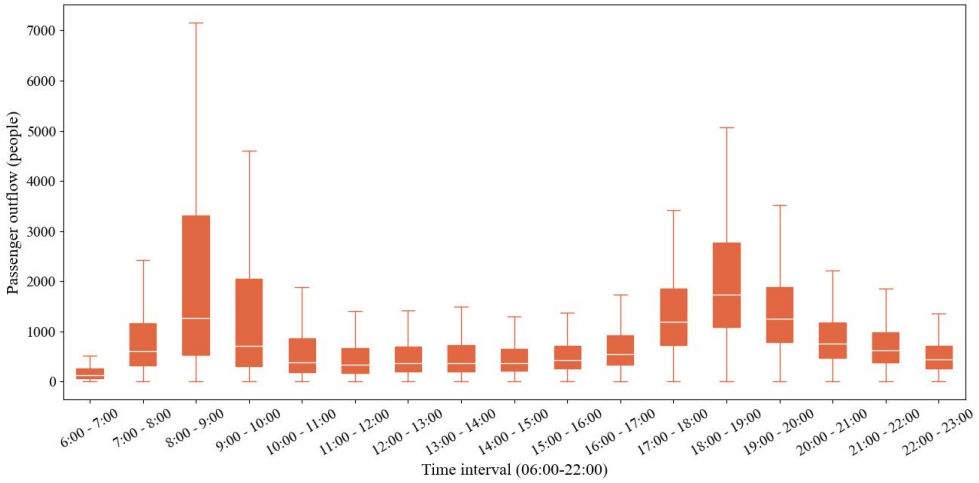

Fig. 3. Passenger outflow at different time intervals on weekdays.

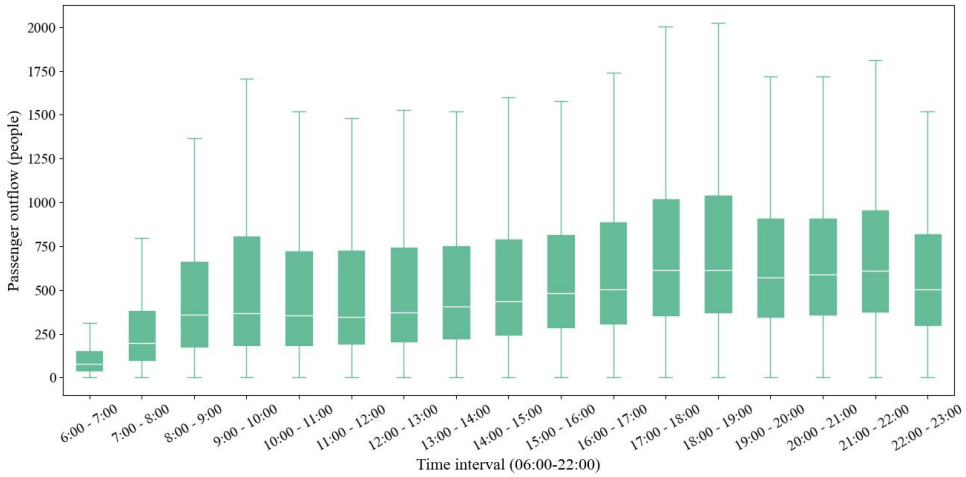

Fig. 4. Passenger outflow at different time intervals on weekends.

Land use characteristics around each station were also integral to the dataset. Points of Interest (POIs) within a 1 km radius of each station were categorized into five main types: commercial, work, residential, education, medical, and commercial POIs made up approximately 65% of the total, reflecting the significant influence of commercial activities on metro passenger flow patterns. Work-related POIs contributed about 19%, residential 8%, educational 5%, and medical POIs 3%. The dataset also includes information on stations' proximity to key areas such as Central Business Districts (CBDs), universities, and transportation hubs, which are expected to have a substantial impact on passenger flows.

5.2 Parameters and experimental settings

The experimental setup for the proposed CSP-AIT-Net model was designed to optimize model performance while maintaining computational efficiency. A systematic selection of hyperparameters was undertaken, incorporating empirical tuning and best practices from the literature.

The Adam optimizer was employed with a learning rate of 1e-3. This value was chosen for its balance between stable convergence and efficient training, as demonstrated in similar prediction tasks. Preliminary tests indicated that lower learning rates, such as 1e-4, led to slower convergence, while higher rates, like 1e-2, caused instability in model training.

A batch size of 128 was selected to strike an optimal balance between training efficiency and resource usage. Larger batch sizes were avoided due to their significant memory demands, which could hinder scalability, while smaller batches introduced excessive variance in the gradient updates. The chosen batch size is consistent with similar large-scale transportation prediction studies, where it provides sufficient

statistical representation without compromising model efficiency.

The embedding dimension for station semantics was set to 128, following insights from prior research that suggest this dimensionality is adequate for representing key station features while avoiding excessive model complexity. This choice allows the model to capture spatial dependencies effectively, including the relationships between stations within proximity, while maintaining manageable computational demands.

The masking mechanism employed 80 flow backtracking instances, reflecting the Pareto principle where a small subset of OD pairs accounts for the majority of passenger flows. It was chosen after testing several options between 50 and 100, with 80 found to provide the best balance between computational efficiency and prediction accuracy.

For the loss function, OD flow prediction loss was weighted at 0.9, while inflow consistency loss was assigned a weight of 0.1. This weighting scheme was based on empirical observations, which showed that emphasizing OD flow prediction led to more impactful operational improvements, while still preserving flow conservation as a secondary constraint.

The model was trained for 100 epochs, with early stopping applied if the validation loss did not improve for 10 consecutive epochs, thus preventing overfitting and ensuring robust generalization. A dropout rate of 0.3 was used as an additional regularization technique to enhance model robustness.

The experiments were conducted using Python 3.8.17 and PyTorch 2.0.0+cu117, running on an NVIDIA GeForce RTX 3050 GPU with 12 GB of memory. This computational setup was selected for its ability to efficiently manage the model's

complexity and the large dataset, enabling timely training and real-time prediction capabilities.

5.3 Comparable methods

Autoregressive Integrated Moving Average (ARIMA) is a widely used method for time series forecasting that models the relationship between a variable and its lagged values, as well as past forecast errors. It combines autoregressive (AR) terms, moving average (MA) terms, and a differencing operation to make the time series stationary.

Random Forest (RF) is an ensemble machine learning method that constructs multiple decision trees during training and outputs the mode of the predictions for classification or the mean prediction for regression. By aggregating predictions from numerous trees, RF improves model accuracy and reduces overfitting.

Gradient Boosting Decision Trees (GBDT) is another ensemble learning method that builds a series of decision trees sequentially, where each tree attempts to correct the errors of the previous one. GBDT has been widely applied to metro passenger flow prediction, offering flexibility in modeling complex non-linear relationships and interactions between various features.

Long Short-Term Memory (LSTM) is a type of recurrent neural network (RNN) designed to model sequential data with long-range dependencies. LSTM addresses the vanishing gradient problem of traditional RNNs by introducing memory cells that store information over long sequences.

Gated Recurrent Unit (GRU) is a simpler variant of LSTM, designed to improve computational efficiency while maintaining the ability to capture long-term temporal dependencies. GRU achieves this by using a simplified gating mechanism,

which combines the forget and input gates into a single update gate.

Hypergraph Neural Network (HGNN) introduces a novel representation of metro networks through the use of hypergraphs, which extend traditional graph theory by allowing connections to involve multiple nodes simultaneously (Wang *et al.*, 2021). This method improves upon standard graph convolution models by capturing higher-order spatial relationships and more complex passenger travel patterns. Hypergraph convolution and spatiotemporal blocks are employed to jointly model the spatial and temporal dependencies, making the HGNN particularly suited for dynamic, large-scale metro systems with intricate passenger flow interactions.

The Space-Time Adaptive Network (STAN) is a deep learning model designed for OD demand prediction by combining edge-based embeddings to represent spatial relationships and adapting temporal features to capture periodic passenger flow patterns (Xu *et al.*, 2024). The model utilizes a global receptive field for spatial interactions, allowing it to preserve fine-grained relations between regions. The prompter mechanism dynamically adjusts temporal parameters, ensuring the model learns periodicity while differentiating between similar and dissimilar periods.

Split-Attention Relational Graph Convolutional Network (SARGCN) is an advanced method that constructs a metro knowledge graph based on OD matrices and land-use features, integrating relational graph convolution and LSTM to model spatiotemporal dependencies in passenger flow (Zeng and Tang, 2023). SARGCN improves upon traditional GCNs by using a split-attention mechanism to dynamically adjust the attention weights given to different relational graph features. This enables the model to learn fine-grained spatiotemporal correlations between stations and effectively capture the interdependencies between passenger inflows and outflows.

Adaptive Feature Fusion Network (AFFN) is a deep learning model designed

to address the challenges of OD passenger flow prediction by adaptively fusing spatial dependencies from multiple knowledge-based graphs and external factors (Xu *et al.*, 2023). The model leverages graph-based representations to capture spatial correlations between metro stations and integrates external features such as land use and weather. By learning the impact of external factors on passenger flow patterns, AFFN enhances the model's ability to make accurate predictions in the presence of sparse data.

6. Results analysis

6.1 Model performance

The analysis of metro passenger flow prediction models in Tables 2 and 3, using the Mean Absolute Percentage Error (MAPE) metric across prediction intervals of 10, 20, 30, and 60 minutes, provides a clear assessment of model robustness and scalability. As prediction intervals lengthen, MAPE values generally increase. Notably, CSP-AIT-Net consistently maintains lower MAPE values compared to other models, with MAPE rising from 36.019% at 10 minutes to 38.483% at 30 minutes, and then to 43.460% at 60 minutes. This performance demonstrates CSP-AIT-Net's robustness, particularly in adapting to long time intervals, where other models exhibit larger errors.

For example, at the 10-minute prediction interval, models can be categorized into traditional (ARIMA), machine learning (RF, GBDT), and deep learning (LSTM, GRU, HGNN, STAN, SARGCN, AFFN, CSP-AIT-Net). ARIMA, with the highest MAPE (69.554%), is clearly limited in capturing complex passenger flow dynamics. Machine learning models, such as RF and GBDT, show moderate improvement with MAPE values of 52.001% and 51.590%, respectively, yet they still struggle with the

intricacies of spatiotemporal dependencies inherent in metro systems.

Deep learning models markedly outperform both traditional and machine learning approaches, demonstrating their strength in capturing temporal and spatial complexities. LSTM and GRU achieved improved MAPE values of 47.237% and 45.617%, respectively, leveraging their ability to model sequential data. However, graph-based deep learning models (HGNN, STAN, SARGCN, AFFN, CSP-AIT-Net) further advance performance by incorporating spatial relationships and interdependencies. Among these, CSP-AIT-Net achieves the lowest MAPE of 36.019%, showcasing its ability to effectively model the multifaceted spatial-temporal dynamics of metro passenger flows.

Graph-based models offer varying levels of improvement, with HGNN yielding a MAPE of 43.571% by capturing higher-order spatial relationships through hypergraphs. STAN, utilizing edge-based embeddings and a global receptive field, achieves a MAPE of 40.252%, effectively adapting to evolving passenger dynamics. SARGCN employs split-attention mechanisms to focus on relevant relational features, resulting in a MAPE of 39.282%. AFFN further enhances accuracy by adaptively fusing spatial dependencies with external contextual factors, achieving a MAPE of 37.491%. Despite these advances, CSP-AIT-Net surpasses all other models, indicating its superior capacity for capturing complex, asynchronous interactions across the metro network.

Table 2. Prediction accuracy comparison among algorithms and intervals (traditional methods).

Metric	Interval	ARIMA	RF	GBDT	LSTM	GRU
MAE	10 min	3.551	2.655	2.634	2.412	2.329
	20 min	7.431	5.556	5.512	5.047	4.874
	30 min	12.588	9.412	9.337	8.549	8.256
	60 min	20.866	15.600	15.477	14.171	13.685
MAPE	10 min	69.554	52.001	51.590	47.237	45.617
	20 min	71.030	53.104	52.685	48.240	46.585

	30 min	74.312	55.558	55.120	50.469	48.738
	60 min	83.923	62.744	62.248	56.996	55.041
RMSE	10 min	4.469	3.341	3.315	3.035	2.931
	20 min	9.327	6.973	6.918	6.335	6.117
	30 min	15.932	11.911	11.817	10.820	10.449
	60 min	26.124	19.531	19.377	17.742	17.133

Table 3. Prediction accuracy comparison among algorithms and intervals (recent studies).

Metric	Interval	HGNN	STAN	SARGCN	AFFN	CSP-AIT-Net
MAE	10 min	2.225	2.055	2.006	1.914	1.839
	20 min	4.655	4.301	4.197	4.006	3.848
	30 min	7.886	7.285	7.110	6.785	6.519
	60 min	13.071	12.075	11.785	11.247	10.806
MAPE	10 min	43.571	40.252	39.282	37.491	36.019
	20 min	44.496	41.106	40.116	38.287	36.783
	30 min	46.552	43.005	41.969	40.056	38.483
	60 min	52.573	48.567	47.397	45.237	43.460
RMSE	10 min	2.800	2.586	2.524	2.409	2.314
	20 min	5.843	5.398	5.268	5.028	4.830
	30 min	9.980	9.220	8.998	8.587	8.250
	60 min	16.365	15.118	14.754	14.082	13.529

6.2 Performance on the spatial and temporal domain

The analysis of the prediction accuracy of Origin-Destination (OD) passenger flow across different spatial regions and temporal periods reveals distinct trends. As shown in Fig 5., for metro stations near universities and work-related areas, passenger flow patterns exhibit greater regularity due to the consistent nature of activities. University regions, for instance, follow a predictable schedule of classes and activities, resulting in stable flow patterns that are easier to model. Similarly, the underlying regularity in commuting behavior enhances the predictability of stations in work-related areas.

Conversely, areas characterized by mixed land use, such as Central Business Districts (CBDs) and transportation hubs, present more complexity in passenger flow dynamics. The diversity of activities in CBDs—ranging from business, and retail, to leisure—leads to high variability in flow patterns, which makes prediction

challenging. Transportation hubs also serve as converging points for different types of trips, leading to a fluctuating and dynamic flow that lacks the regularity observed in other areas. The inherent irregularity in such mixed-use regions results in higher prediction errors, as the passenger flows are driven by a broader range of factors, including events, varying trip purposes, and changing schedules.

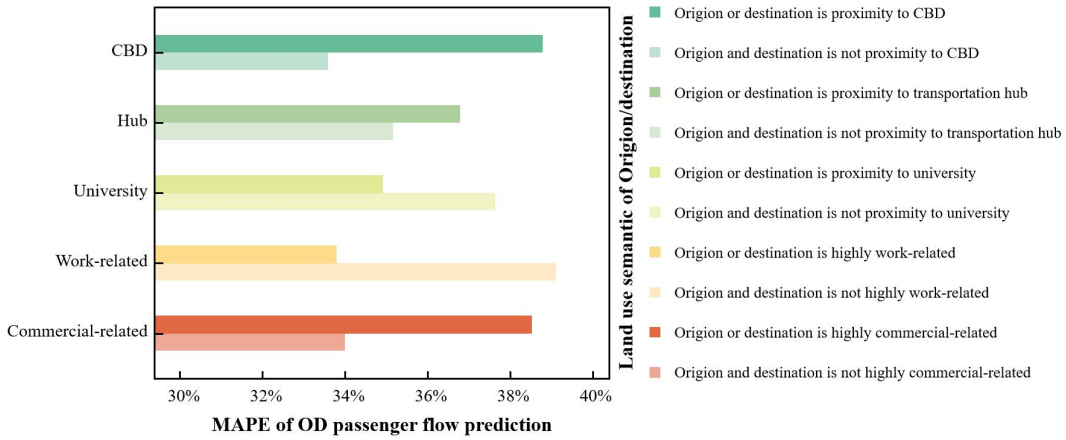

Fig. 5. Comparison of prediction accuracy among different land use semantics (10 minutes).

Temporal analysis further reveals important trends in how prediction accuracy varies throughout the day. The passenger flow exhibits a clear U-shaped pattern, with higher variability and errors during the morning and evening rush hours, and more regular flow patterns around midday. This phenomenon could be attributed to reduced travel during midday, resulting in smaller fluctuations in passenger flow. Additionally, prediction results across different days of the week also show a certain regularity, with higher prediction accuracy on weekdays compared to weekends. This is likely due to more commuting trips on weekdays, which are inherently more predictable.

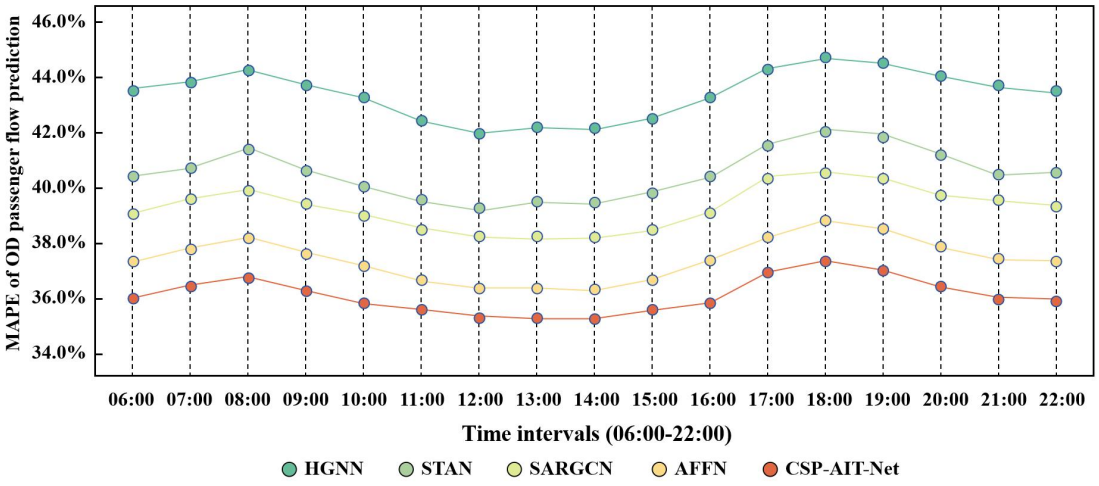

Fig. 6. Prediction accuracy comparison among algorithms at various time intervals (10 minutes).

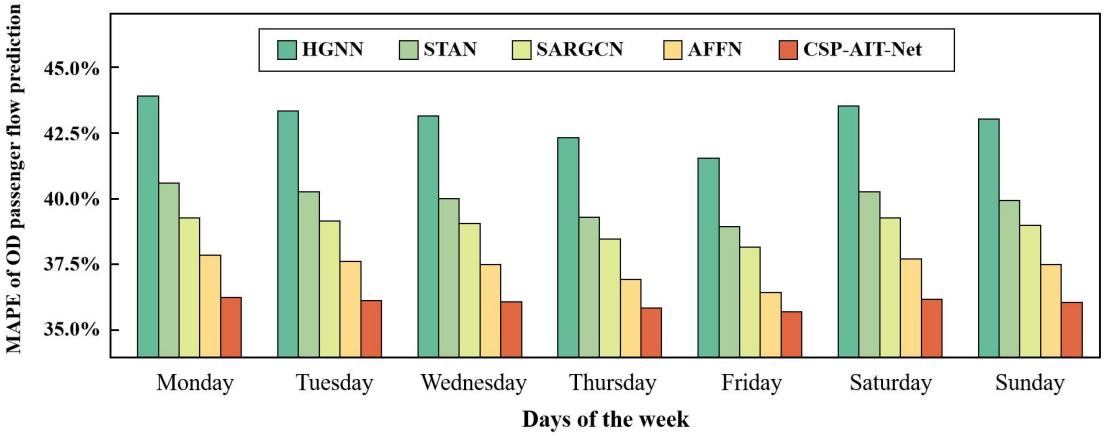

Fig. 7. Prediction accuracy comparison among algorithms from Monday to Sunday (10 minutes).

6.3 Ablation analysis

The ablation study in Tables 4, 5, and 6 highlights the necessity of three key components in CSP-AIT-Net: graph contrastive learning, asynchronous inflow, and the graph attention mechanism. These components significantly enhance model accuracy and robustness. Graph contrastive learning effectively enhances station semantic extraction. Without semantic attributes, the MAPE at the 10-minute interval is 47.245%, decreasing to 38.758% with basic encoding and 36.019% with graph contrastive learning. The consistent reduction across intervals demonstrates its role in capturing complex spatial features, leading to lower prediction errors.

Table 4. Prediction accuracy comparison on station semantic extraction.

Metric	Interval	No land use attributes	Basic encoding	Graph contrastive learning
MAE	10 min	2.412	1.979	1.839
	20 min	5.048	4.141	3.848
	30 min	8.551	7.015	6.519
	60 min	14.173	11.627	10.806
MAPE	10 min	47.245	38.758	36.019
	20 min	48.247	39.581	36.783
	30 min	50.477	41.410	38.483
	60 min	57.005	46.765	43.460
RMSE	10 min	3.036	2.490	2.314
	20 min	6.336	5.198	4.830
	30 min	10.821	8.878	8.250
	60 min	17.745	14.557	13.529

Asynchronous inflow consideration is crucial for accurate modeling, as shown in Table 5. Ignoring asynchronous inflows results in a MAPE of 40.103% at the 10-minute interval, while incorporating them reduces it to 36.019%, demonstrating the importance of modeling temporal inconsistencies in passenger flow mobility.

Table 5. Prediction accuracy comparison on asynchronous inflow.

Metric	Interval	No asynchronous inflow	Considering asynchronous inflow
MAE	10 min	2.048	1.839
	20 min	4.285	3.848
	30 min	7.258	6.519
	60 min	12.031	10.806
MAPE	10 min	40.103	36.019
	20 min	40.954	36.783
	30 min	42.847	38.483
	60 min	48.388	43.460
RMSE	10 min	2.577	2.314
	20 min	5.378	4.830
	30 min	9.186	8.250
	60 min	15.063	13.529

The Graph Attention mechanism further refines accuracy by dynamically prioritizing relevant spatial and temporal dependencies. Without graph attention, the MAPE at the 10-minute interval is 46.147%, dropping to 36.019% when included. This mechanism allows CSP-AIT-Net to focus on critical OD pairs, improving prediction accuracy across all intervals.

Table 6. Prediction accuracy comparison on spatiotemporal graph attention mechanism.

Metric	Interval	No graph attention	Considering graph attention
MAE	10 min	2.356	1.839
	20 min	4.930	3.848
	30 min	8.352	6.519
	60 min	13.844	10.806
MAPE	10 min	46.147	36.019
	20 min	47.127	36.783
	30 min	49.305	38.483
	60 min	55.681	43.460
RMSE	10 min	2.965	2.314
	20 min	6.188	4.830
	30 min	10.570	8.250
	60 min	17.333	13.529

7. Conclusion

This study proposed CSP-AIT-Net, a contrastive learning-enhanced spatiotemporal graph attention framework for short-term metro OD passenger flow prediction with asynchronous inflow tracking. The proposed framework significantly improved OD flow prediction accuracy by capturing the asynchronous characteristics of metro flows and integrating inflow and outflow data into a unified prediction model. The contrastive learning allows the model to better capture complex contextual patterns related to land use and passenger mobility. Experimental results on real-world metro datasets demonstrated that CSP-AIT-Net consistently outperformed state-of-the-art methods, achieving lower prediction errors across various time intervals and reducing the MAPE by over 4% compared to the best-performing existing models.

The innovation of CSP-AIT-Net lies in its integration of asynchronous inflow tracking, spatiotemporal graph attention, and contrastive learning for enhanced semantic representation of metro stations. Unlike traditional models that neglect temporal misalignment between inflows and outflows, our framework directly

addresses this by incorporating asynchronous inflow graphs, providing a more granular understanding of OD dynamics, particularly for irregular passenger movements. The use of contrastive learning enabled the effective extraction of high-dimensional features, representing relationships between stations. These innovations collectively address gaps in current OD-level passenger flow prediction research.

Despite these advancements, several limitations of CSP-AIT-Net still remain. Future research could extend the framework to multi-step forecasting for better long-term analysis. Additionally, integrating detailed individual trip plans from the MaaS app could further improve accuracy. Exploring model scalability in complex metro systems and integrating data from other transportation modes could provide a holistic view of urban mobility, enhancing coordinated transit management.

References

Chen, E., Ye, Z., Wang, C., & Xu, M. (2020). Subway Passenger Flow Prediction for Special Events Using Smart Card Data. *IEEE Transactions on Intelligent Transportation Systems, 21*(3), 1109-1120. doi:10.1109/TITS.2019.2902405

Chen, P., Fu, X., & Wang, X. (2022). A Graph Convolutional Stacked Bidirectional Unidirectional-LSTM Neural Network for Metro Ridership Prediction. *IEEE Transactions on Intelligent Transportation Systems, 23*(7), 6950-6962. doi:10.1109/TITS.2021.3065404

Cheng, J., Liu, G., Gao, S., Raza, A., Li, J., & Juan, W. (2024). Short-Term Passenger Flow Prediction in Urban Rail Transit Based on Points of Interest. *IEEE Access, 12*, 95196-95208. doi:10.1109/ACCESS.2024.3425634

Du, B., Peng, H., Wang, S., Bhuiyan, M. Z. A., Wang, L., Gong, Q., . . . Li, J. (2020). Deep Irregular Convolutional Residual LSTM for Urban Traffic Passenger Flows Prediction. *IEEE Transactions on Intelligent Transportation Systems, 21*(3), 972-985. doi:10.1109/TITS.2019.2900481

Du, Q., Zhou, Y., Huang, Y., Wang, Y., & Bai, L. (2022). Spatiotemporal exploration of the non-linear impacts of accessibility on metro ridership. *Journal of Transport Geography, 102*, 103380. doi:https://doi.org/10.1016/j.jtrangeo.2022.103380

Fang, S., Prinet, V., Chang, J., Werman, M., Zhang, C., Xiang, S., & Pan, C. (2022). MS-Net: Multi-Source Spatio-Temporal Network for Traffic Flow Prediction. *IEEE Transactions on Intelligent Transportation Systems, 23*(7), 7142-7155. doi:10.1109/TITS.2021.3067024

Fang, S., Zhang, C., Xiang, S., & Pan, C. (2023). AutoMSNet: Multi-Source Spatio-Temporal Network

via Automatic Neural Architecture Search for Traffic Flow Prediction. *IEEE Transactions on Intelligent Transportation Systems, 24*(3), 2827-2841. doi:10.1109/TITS.2022.3225553

Fang, S., Zhang, Q., Meng, G., Xiang, S., & Pan, C. (2019). *GSTNet: Global spatial-temporal network for traffic flow prediction.* Paper presented at the IJCAI.

Hasselwander, M., Bigotte, J. F., Antunes, A. P., & Sigua, R. G. (2022). Towards sustainable transport in developing countries: Preliminary findings on the demand for mobility-as-a-service (MaaS) in Metro Manila. *Transportation Research Part A: Policy and Practice, 155*, 501-518. doi:https://doi.org/10.1016/j.tra.2021.11.024

Hoogervorst, R., Dollevoet, T., Maróti, G., & Huisman, D. (2020). Reducing Passenger Delays by Rolling Stock Rescheduling. *Transportation Science, 54*(3), 762-784. doi:10.1287/trsc.2019.0968

Huang, H., Mao, J., Lu, W., Hu, G., & Liu, L. (2023). DEASeq2Seq: An attention based sequence to sequence model for short-term metro passenger flow prediction within decomposition-ensemble strategy. *Transportation Research Part C: Emerging Technologies, 146*, 103965. doi:https://doi.org/10.1016/j.trc.2022.103965

Jiang, W., Ma, Z., & Koutsopoulos, H. N. (2022). Deep learning for short-term origin–destination passenger flow prediction under partial observability in urban railway systems. *Neural Computing and Applications, 34*(6), 4813-4830. doi:10.1007/s00521-021-06669-1

Jiao, P., Li, R., Sun, T., Hou, Z., & Ibrahim, A. (2016). Three Revised Kalman Filtering Models for Short-Term Rail Transit Passenger Flow Prediction. *Mathematical Problems in Engineering, 2016*(1), 9717582. doi:https://doi.org/10.1155/2016/9717582

Li, C., Huang, J., Wang, B., Zhou, Y., Bai, Y., & Chen, Y. (2019). Spatial-Temporal Correlation Prediction Modeling of Origin-Destination Passenger Flow Under Urban Rail Transit Emergency Conditions. *IEEE Access, 7*, 162353-162365. doi:10.1109/ACCESS.2019.2951604

Lin, D., Broere, W., & Cui, J. (2022). Metro systems and urban development: Impacts and implications. *Tunnelling and Underground Space Technology, 125*, 104509. doi:https://doi.org/10.1016/j.tust.2022.104509

Liu, J., Jiang, R., Zhu, D., & Zhao, J. (2022). Short-Term Subway Inbound Passenger Flow Prediction Based on AFC Data and PSO-LSTM Optimized Model. *Urban Rail Transit, 8*(1), 56-66. doi:10.1007/s40864-022-00166-x

Liu, L., Zhu, Y., Li, G., Wu, Z., Bai, L., & Lin, L. (2023). Online Metro Origin-Destination Prediction via Heterogeneous Information Aggregation. *IEEE Transactions on Pattern Analysis and Machine Intelligence, 45*(3), 3574-3589. doi:10.1109/TPAMI.2022.3178184

Liu, Y., Liu, Z., & Jia, R. (2019). DeepPF: A deep learning based architecture for metro passenger flow prediction. *Transportation Research Part C: Emerging Technologies, 101*, 18-34. doi:https://doi.org/10.1016/j.trc.2019.01.027

Lu, Y., Ding, H., Ji, S., Sze, N. N., & He, Z. (2021). Dual attentive graph neural network for metro passenger flow prediction. *Neural Computing and Applications, 33*(20), 13417-13431. doi:10.1007/s00521-021-05966-z

Lu, Y., Yang, L., Yang, H., Zhou, H., & Gao, Z. (2023). Robust collaborative passenger flow control on a congested metro line: A joint optimization with train timetabling. *Transportation Research Part B: Methodological, 168*, 27-55. doi:https://doi.org/10.1016/j.trb.2022.12.008

Lv, S., Wang, K., Yang, H., & Wang, P. (2024). An origin–destination passenger flow prediction system

based on convolutional neural network and passenger source-based attention mechanism. *Expert Systems with Applications, 238*, 121989. doi:https://doi.org/10.1016/j.eswa.2023.121989

Ma, C., Zhang, B., Li, S., & Lu, Y. (2024). Urban rail transit passenger flow prediction with ResCNN-GRU based on self-attention mechanism. *Physica A: Statistical Mechanics and its Applications, 638*, 129619. doi:https://doi.org/10.1016/j.physa.2024.129619

Ma, X., Zhang, J., Du, B., Ding, C., & Sun, L. (2019). Parallel Architecture of Convolutional Bi-Directional LSTM Neural Networks for Network-Wide Metro Ridership Prediction. *IEEE Transactions on Intelligent Transportation Systems, 20*(6), 2278-2288. doi:10.1109/TITS.2018.2867042

Mandhani, J., Nayak, J. K., & Parida, M. (2021). Establishing service quality interrelations for Metro rail transit: Does gender really matter? *Transportation Research Part D: Transport and Environment, 97*, 102888. doi:https://doi.org/10.1016/j.trd.2021.102888

Mo, P., Yang, L., Wang, Y., & Qi, J. (2019). A flexible metro train scheduling approach to minimize energy cost and passenger waiting time. *Computers & Industrial Engineering, 132*, 412-432. doi:https://doi.org/10.1016/j.cie.2019.04.031

Ou, J., Sun, J., Zhu, Y., Jin, H., Liu, Y., Zhang, F., . . . Wang, X. (2023). STP-TrellisNets+: Spatial-Temporal Parallel TrellisNets for Multi-Step Metro Station Passenger Flow Prediction. *IEEE Transactions on Knowledge and Data Engineering, 35*(7), 7526-7540. doi:10.1109/TKDE.2022.3187690

Roos, J., Gavin, G., & Bonnevay, S. (2017). A dynamic Bayesian network approach to forecast short-term urban rail passenger flows with incomplete data. *Transportation Research Procedia, 26*, 53-61. doi:https://doi.org/10.1016/j.trpro.2017.07.008

Shen, L., Li, J., Chen, Y., Li, C., Chen, X., & Lee, D. H. (2024). Short-Term Metro Origin-Destination Passenger Flow Prediction via Spatio-Temporal Dynamic Attentive Multi-Hypergraph Network. *IEEE Transactions on Intelligent Transportation Systems, 25*(8), 9945-9957. doi:10.1109/TITS.2024.3359763

Shen, L., Shao, Z., Yu, Y., & Chen, X. (2021). Hybrid Approach Combining Modified Gravity Model and Deep Learning for Short-Term Forecasting of Metro Transit Passenger Flows. *Transportation Research Record, 2675*(1), 25-38. doi:10.1177/0361198120968823

Shi, Z., Zhang, N., Schonfeld, P. M., & Zhang, J. (2020). Short-term metro passenger flow forecasting using ensemble-chaos support vector regression. *Transportmetrica A: Transport Science, 16*(2), 194-212. doi:10.1080/23249935.2019.1692956

Su, H., Mo, S., Dai, H., & Shen, J. (2024). Short-Term Prediction of Origin–Destination Passenger Flow in Urban Rail Transit Systems with Multi-Source Data: A Deep Learning Method Fusing High-Dimensional Features. *Mathematics, 12*(20), 3204.

Tang, L., Zhao, Y., Cabrera, J., Ma, J., & Tsui, K. L. (2019). Forecasting Short-Term Passenger Flow: An Empirical Study on Shenzhen Metro. *IEEE Transactions on Intelligent Transportation Systems, 20*(10), 3613-3622. doi:10.1109/TITS.2018.2879497

Teng, J., Pan, W., & Zhang, C. (2020). Quantitative Modeling of Congestion in Metro Station Based on Passenger Time Perceptions. *Transportation Research Record, 2674*(5), 270-281. doi:10.1177/0361198120914900

Toqué, F., Khouadjia, M., Come, E., Trepanier, M., & Oukhellou, L. (2017, 16-19 Oct. 2017). *Short & long term forecasting of multimodal transport passenger flows with machine learning methods.*

Paper presented at the 2017 IEEE 20th International Conference on Intelligent Transportation Systems (ITSC).

Wang, J., Leng, B., Wu, J., Du, H., & Xiong, Z. (2020). MetroEye: A Weather-Aware System for Real-Time Metro Passenger Flow Prediction. *IEEE Access, 8*, 129813-129829. doi:10.1109/ACCESS.2020.3007538

Wang, J., Zhang, Y., Wei, Y., Hu, Y., Piao, X., & Yin, B. (2021). Metro passenger flow prediction via dynamic hypergraph convolution networks. *IEEE Transactions on Intelligent Transportation Systems, 22*(12), 7891-7903.

Wei, Y., & Chen, M.-C. (2012). Forecasting the short-term metro passenger flow with empirical mode decomposition and neural networks. *Transportation Research Part C: Emerging Technologies, 21*(1), 148-162. doi:https://doi.org/10.1016/j.trc.2011.06.009

Xu, H., Chen, Y., Li, C., & Chen, X. M. (2024). Space-Time adaptive network for origin-destination passenger demand prediction. *Transportation Research Part C: Emerging Technologies, 167*, 104842.

Xu, X., Lu, Y., Wang, Y., Li, J., & Zhang, H. (2020). Improving Service Quality of Metro Systems—A Case Study in the Beijing Metro. *IEEE Access, 8*, 12573-12591. doi:10.1109/ACCESS.2020.2965990

Xu, Y., Lyu, Y., Xiong, G., Wang, S., Wu, W., Cui, H., & Luo, J. (2023). Adaptive Feature Fusion Networks for Origin-Destination Passenger Flow Prediction in Metro Systems. *IEEE Transactions on Intelligent Transportation Systems, 24*(5), 5296-5312. doi:10.1109/TITS.2023.3239101

Yan, D., Zhou, J., Zhao, Y., & Wu, B. (2018, 2018//). *Short-Term Subway Passenger Flow Prediction Based on ARIMA.* Paper presented at the Geo-Spatial Knowledge and Intelligence, Singapore.

Yang, C., Yu, C., Dong, W., & Yuan, Q. (2023). Substitutes or complements? Examining effects of urban rail transit on bus ridership using longitudinal city-level data. *Transportation Research Part A: Policy and Practice, 174*, 103728. doi:https://doi.org/10.1016/j.tra.2023.103728

Yang, J., Han, X., Ye, T., Tang, Y., Feng, W., Wang, A., . . . Zhang, Q. (2022). Spatiotemporal Virtual Graph Convolution Network for Key Origin-Destination Flow Prediction in Metro System. *Mathematical Problems in Engineering, 2022*(1), 5622913. doi:https://doi.org/10.1155/2022/5622913

Yang, Y., Zhang, J., Yang, L., Yang, Y., Li, X., & Gao, Z. (2023). Short-term passenger flow prediction for multi-traffic modes: A Transformer and residual network based multi-task learning method. *Information Sciences, 642*, 119144. doi:https://doi.org/10.1016/j.ins.2023.119144

Yin, D., Jiang, R., Deng, J., Li, Y., Xie, Y., Wang, Z., . . . Shang, J. S. (2023). MTMGNN: Multi-time multi-graph neural network for metro passenger flow prediction. *GeoInformatica, 27*(1), 77-105. doi:10.1007/s10707-022-00466-1

Zeng, J., & Tang, J. (2023). Combining knowledge graph into metro passenger flow prediction: A split-attention relational graph convolutional network. *Expert Systems with Applications, 213*, 118790. doi:https://doi.org/10.1016/j.eswa.2022.118790

Zhan, S., Cai, Y., Xiu, C., Zuo, D., Wang, D., & Chun Wong, S. (2024). Parallel framework of a multi-graph convolutional network and gated recurrent unit for spatial–temporal metro passenger flow prediction. *Expert Systems with Applications, 251*, 123982. doi:https://doi.org/10.1016/j.eswa.2024.123982

Zhang, J., Chen, F., Cui, Z., Guo, Y., & Zhu, Y. (2021). Deep Learning Architecture for Short-Term

Passenger Flow Forecasting in Urban Rail Transit. *IEEE Transactions on Intelligent Transportation Systems, 22*(11), 7004-7014. doi:10.1109/TITS.2020.3000761

Zhang, Y., Sun, K., Wen, D., Chen, D., Lv, H., & Zhang, Q. (2023). Deep Learning for Metro Short-Term Origin-Destination Passenger Flow Forecasting Considering Section Capacity Utilization Ratio. *IEEE Transactions on Intelligent Transportation Systems, 24*(8), 7943-7960. doi:10.1109/TITS.2023.3266371

Zhao, Y., Ma, Z., Yang, Y., Jiang, W., & Jiang, X. (2020). Short-Term Passenger Flow Prediction With Decomposition in Urban Railway Systems. *IEEE Access, 8*, 107876-107886. doi:10.1109/ACCESS.2020.3000242

Zheng, F., Zhao, J., Ye, J., Gao, X., Ye, K., & Xu, C. (2023). Metro OD Matrix Prediction Based on Multi-View Passenger Flow Evolution Trend Modeling. *IEEE Transactions on Big Data, 9*(3), 991-1003. doi:10.1109/TBDATA.2022.3229836